Grid-Following Inverters and Synchronous Condensers: A Grid-Forming Pair?

Preprint

Rick Wallace Kenyon,[1,2] Anderson Hoke,[1,2] Jin Tan,[2] Benjamin Kroposki,[2] and Bri-Mathias Hodge[1,2]

[1] *University of Colorado, Boulder*
[2] *National Renewable Energy Laboratory*

Presented at the 2020 Clemson University Power Systems Conference
Clemson, South Carolina
March 10–13, 2020

NREL is a national laboratory of the U.S. Department of Energy
Office of Energy Efficiency & Renewable Energy
Operated by the Alliance for Sustainable Energy, LLC

This report is available at no cost from the National Renewable Energy Laboratory (NREL) at www.nrel.gov/publications.

Contract No. DE-AC36-08GO28308

Conference Paper
NREL/CP-5D00-75848
March 2020

Grid-Following Inverters and Synchronous Condensers: A Grid-Forming Pair?

Preprint

Rick Wallace Kenyon,[1,2] Anderson Hoke,[1,2] Jin Tan,[2] Benjamin Kroposki,[2] and Bri-Mathias Hodge[1,2]

[1] *University of Colorado, Boulder*
[2] *National Renewable Energy Laboratory*

Suggested Citation
Kenyon, Rick Wallace, Anderson Hoke, Jin Tan, Benjamin Kroposki, and Bri-Mathias Hodge. 2020. *Grid-Following Inverters and Synchronous Condensers: A Grid-Forming Pair?: Preprint*. Golden, CO: National Renewable Energy Laboratory. NREL/CP-5D00-75848. https://www.nrel.gov/docs/fy20osti/75848.pdf.

NREL is a national laboratory of the U.S. Department of Energy
Office of Energy Efficiency & Renewable Energy
Operated by the Alliance for Sustainable Energy, LLC

This report is available at no cost from the National Renewable Energy Laboratory (NREL) at www.nrel.gov/publications.

Contract No. DE-AC36-08GO28308

Conference Paper
NREL/CP-5D00-75848
March 2020

National Renewable Energy Laboratory
15013 Denver West Parkway
Golden, CO 80401
303-275-3000 • www.nrel.gov

NOTICE

This work was authored in part by the National Renewable Energy Laboratory, operated by Alliance for Sustainable Energy, LLC, for the U.S. Department of Energy (DOE) under Contract No. DE-AC36-08GO28308.Funding provided by U.S. Department of Energy Office of Energy Efficiency and Renewable Energy Solar Energy Technologies Office. The views expressed herein do not necessarily represent the views of the DOE or the U.S. Government. The U.S. Government retains and the publisher, by accepting the article for publication, acknowledges that the U.S. Government retains a nonexclusive, paid-up, irrevocable, worldwide license to publish or reproduce the published form of this work, or allow others to do so, for U.S. Government purposes.

Cover Photos by Dennis Schroeder: (clockwise, left to right) NREL 51934, NREL 45897, NREL 42160, NREL 45891, NREL 48097, NREL 46526.

Grid-Following Inverters and Synchronous Condensers: A Grid-Forming Pair?

Rick Wallace Kenyon[1,2], Anderson Hoke[2], Jin Tan[2], Benjamin Kroposki[2], Bri-Mathias Hodge[1,2]
[1]Electrical, Computer, and Energy Engineering; Renewable and Sustainable Energy Institute
University of Colorado Boulder, Boulder, USA
{richard.kenyonjr, brimathias.hodge}@colorado.edu
[2]Power Systems Engineering Center, *National Renewable Energy Laboratory, Golden, USA*
{richard.kenyon, andy.hoke, jin.tan, benjamin.kroposki, bri.mathias.hodge}@nrel.gov

***Abstract*—As power systems across the globe continue to achieve higher instantaneous penetrations of power electronic converter-interfaced renewable sources, the stability of these power systems is challenged because of the removal of synchronous machines, from which stability is traditionally derived. Although technological solutions to these stability challenges are on the horizon, such as the use of grid-forming inverters, they are not yet widely applied to larger power systems, which presents operational challenges for power systems achieving these high instantaneous penetrations today. A potential interim solution using existing technologies is to pair synchronous condensers with grid-following inverters, which might prolong the stability of an operating power system while synchronous generators are turned off during periods of high renewable energy availability. This work examines the transient stability of such a solution using PSCAD simulations of a two-bus system coupled to a varied-length transmission line, with a synchronous condenser at one bus and a grid-following inverter with grid-support functionality at the other. The system is exposed to load step, balanced fault, and unbalanced fault perturbations. It was found that this simple system returned to a steady state for transmission line lengths up to 125 km after 10% load steps, or a variety of fault types.**

***Index Terms*—grid-following inverters, synchronous condensers, PSCAD, inertia**

I. Introduction

In the 21st century, renewable energy sources are being employed in ever-increasing quantities for a variety of environmental, political, and economic reasons [1], [2]. These goals and subsequent achievements are often specified on an annual energy basis; however, power systems achieving even modest renewable energy levels often hit relatively higher instantaneous penetrations [2], as shown in Fig. 1, which is a plot of annual and instantaneous penetrations by system size for synchronous systems of note. The primary technology for interfacing renewable energies, particularly wind and solar, is the power electronics converter (PEC). As a result, these high instantaneous renewable penetrations correlate with high instantaneous PEC penetrations. Because power systems in general are designed and stabilized around the operating characteristics and physics of synchronous generators (SGs), which are distinct from the attributes of PECs, these high penetrations introduce a variety of challenges to the stability and control of the resultant power system [3], [4].

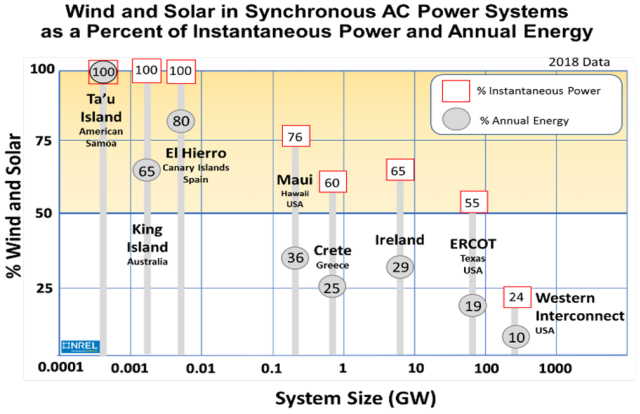

Fig. 1. 2018 annual energy and peak instantaneous penetrations of PECs by system size.

Synchronous condensers (SCs)—synchronous machines without prime movers—have been identified as a complementary technology to some of the challenges associated with high levels of PECs. As the inertia of a power system declines with higher PEC levels [5], which introduces faster dynamics to the system frequency following a load/generation imbalance, SCs can be used to replace some of the inertia lost from SGs [6], [7]. Additionally, SCs can contribute to the short-circuit strength of a power system, which in general declines with high levels of PECs [8]. This can both improve system stability and provide fault current for protection purposes [9].

Another challenge of high PEC levels is the primary approach for integrating PECs with *grid-following* control, in which the PEC tracks an existing sinusoidal AC voltage waveform and injects current according to power set points. At high penetrations of grid-following PECs, general instabilities exist because there are fewer assets "forming" the grid. This is shown via a bears-on-bicycles cartoon in Fig. 2. SMCs form these sinusoidal AC waveforms by design. PECs can be controlled to do so—and they are then considered *grid forming*—via novel control strategies such as droop [10], virtual synchronous machine control [11], and virtual oscillator control [12]. Although these technologies are being used in parts of the world already, they are not yet a standard

application in all power systems indicating the potential need for other solutions.

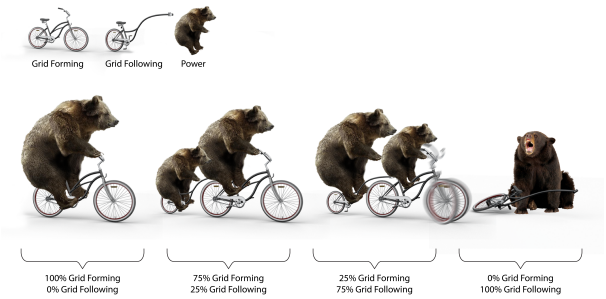

Fig. 2. Bears on bicycles showing conceptually that with high levels of grid-following PECs, the system becomes unstable simply because sufficient levels of grid-forming assets are not present [13]. Here, the full bicycle is any grid-forming asset, either SGs or grid-forming PECs, whereas the tagalong bicycle is a grid-following asset, with or without grid-supporting functionality.

For power systems experiencing high instantaneous PEC penetrations today, and facing the reality that grid-forming PECs are not yet a standard technology in larger power systems, a possible solution is pairing grid-following inverters (GFLs), a type of PEC, and SCs. In this system, the GFLs provide the real power to the system, whereas the SCs provide the sinusoidal AC waveform necessary for the GFLs to track. The proffered solution could allow 100% PEC penetrations for short periods of time—but only after the power system is operational; i.e., this is not a black-start system. The intent of this work is to assess the stability of this pair with electromagnetic transient (EMT) simulations of perturbations, such as load steps and faults, on a small two-bus test system with varying transmission line lengths.

II. Methodology

The applicability of this scenario is to a power system in steady state; i.e., the SC is operating at nominal frequency, and load is being mostly served by the GFL. Such a case is analogous to a power system operating with a surplus of renewable energy (perhaps because of curtailment or because it is stored in a battery energy system) interfaced with the GFL, but with a SG presence. The motivation to disconnect these SGs comes from minimum output constraints; although there is a surplus of renewable energy, some fossil-based consumption will occur because the SGs cannot be ramped down any farther. Under these conditions, it might be advantageous to disconnect the SGs to achieve full renewable energy consumption while the surplus is present. Thus, although the SC and GFL pair is not black-start capable, it is applicable to a power system already in steady state with a renewable energy surplus.

To assess the steady state and transient stability of the GFL and SC system, EMT simulations are performed using PSCAD on a small test system. The system is shown in Fig. 3, where the SC and load are located at Bus 1, and the GFL is located at Bus 2. The length of the single transmission line between them is adjusted to change the electrical distance between the two devices. A basic assumption in these simulations is that sufficient headroom is available for the GFL. This headroom source is not further discussed, but conceptually it might be supplied by methods such as curtailment or a battery energy storage system.

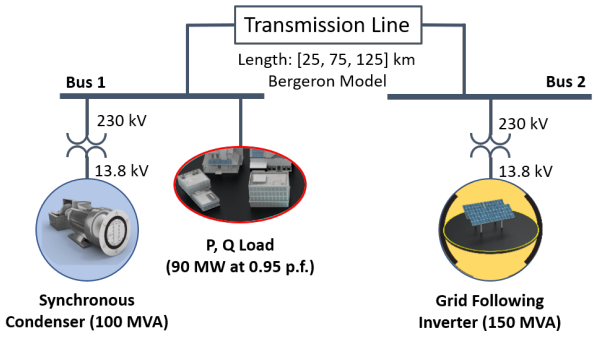

Fig. 3. Two-bus system setup with a grid-following PEC, a synchronous condenser, a constant power load, and a Bergeron model transmission line with varied length. Transformers interface the synchronous condenser and PEC.

The GFL is operated only with a frequency droop functionality, where a change in frequency outside of a deadband results in a modulation of real power output. Fig. 4 shows this relationship between power output and frequency. There is no secondary response to frequency deviations, and as a result the frequency does not return to nominal after the disturbance. For the last set of simulations, unbalanced faults with different line lengths were investigated.

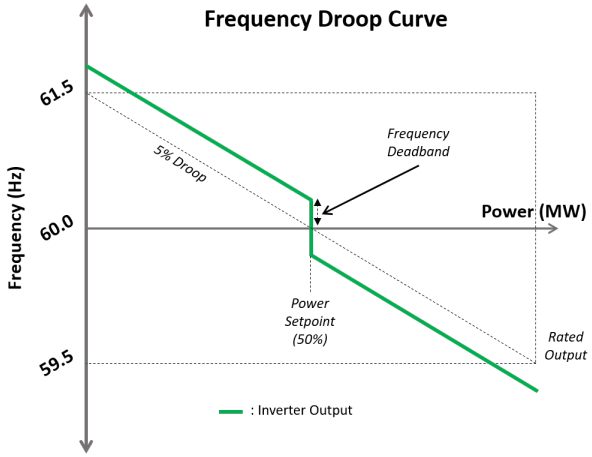

Fig. 4. Frequency droop curve showing the change in real power output based on frequency deviations for a 5% droop. Frequency deadband is visible as the deviation from nominal without a corresponding real power output modulation.

III. Simulation Setup

The test system for these studies is a simple two-bus 230-kV system with a single transmission line interconnect. The transmission line is simulated with a PSCAD Bergeron model,

with the positive-sequence per-length parameters presented in Table I. The zero-sequence parameters are estimated by scaling the positive-sequence parameters; the scaling coefficients were taken from the IEEE 9-bus test system. For the initial sensitivity studies, the line length is set to 25 km. The load for the system is located at the SC bus, and it is modeled as constant power. The load is initially 90 MW operating at a 0.95 power factor (30 Mvar). The 10% load step maintains the 0.95 power factor. When implemented, the fault on the system is applied to the SC bus. It is a bolted (near-zero impedance) fault that clears after six cycles (0.1 s).

TABLE I
POSITIVE-SEQUENCE TRANSMISSION LINE PARAMETERS

Parameter	Unit	Value
R	$m\Omega/m$	0.05
X_L	$m\Omega/m$	0.49
X_C	$Ms*m$	296.65

A. Synchronous Condenser

The SC model in PSCAD consists of a synchronous machine and exciter pair, with no governor or prime mover. The synchronous machine is a generic model with no adjustments made to the generic parameters of the associated machine attributes. The exciter is a solid-state type (SCRX), with a lead/lag filter (time constants of 0.1 s and 0.2 s, respectively) and exciter time constant of 0.065 s. The SC is connected to the 230-kV bus with a 13.8/230-kV delta/grounded wye transformer rated at 200 MVA. The exciter uses the measured per-unit voltage from the transformer high-voltage side as a feedback signal, scaled by the transformer turns ratio and compared to a unity per-unit voltage reference. The control scheme is proportional in nature; the SC does not regulate the voltage. Pertinent ratings of the SC are presented in Table II.

TABLE II
SYNCHRONOUS CONDENSER PARAMETERS

Parameter	Unit	Value
Machine rating	MVA	100
Voltage rating (L-L)	kV	13.8
Inertia constant	s	2
Mechanical friction/windage	p.u.	0.01
Exciter gain	p.u.	5
Max. field voltage	p.u.	5
Min. field voltage	p.u.	-5

In steady state, the SC is a net consumer of real power, the magnitude of which is a factor of a few machine parameters—e.g., mechanical friction, iron loss resistance, armature resistance. No effort was made here to optimize this steady-state consumption, but work has been done on methods to reduce these losses with super conductors, achieving near 99% efficiencies [14]. In these simulations, the efficiency is roughly 98%; i.e., the SC consumes approximately 1.5 MW in steady state of the approximately 92 MW of system load. An inertia constant of $2s$ was selected for the majority of these simulations, which is consistent with the typical SC [8], [14]. A sensitivity study is performed for inertia constants up to $6s$, which is based on the concept of attaching flywheels to the SC to increase the inertia [8].

B. Grid-Following Inverter

The GFL is a user-defined model in PSCAD that controls the output of a three-phase current source. The control is performed in the DQ reference frame, where the transformed v_d and v_q variables are immediately passed through a smoothing low-pass filter (LPF) with a 10-ms time constant. The phase-locked loop used to establish the DQ reference angle has proportional and integral gains of 50 and 900, respectively. The current reference calculations maintain cross coupling; i.e., v_q values are propagated throughout and not assumed to be zero. There is no feed-forward mechanism. Within the power controller, there is a PQ priority mechanism. In all simulations, a P priority is established. Third to the end of the control path, the DQ current commands are passed through a first-order LPF that emulates the response time of the GFL. The time constant in this LPF is varied for the sensitivity studies, but it is otherwise set at 50 ms. It is recognized that this is a rapid response time but still within the capabilities of modern inverters. Second to the end of the control path, an algebraic current-limiting scheme is implemented. The euclidean norm of the DQ currents is measured, and the values are proportionally scaled to meet the DQ current limit if a violation exists. The last item in the control path is the transformation back to the ABC frame, and subsequent current source implementation. Relevant GFL parameters are summarized in Table III

TABLE III
GFL INVERTER PARAMETERS

Parameter	Unit	Value
Machine rating	MVA	150
Voltage rating (L-L)	kV	13.8
Frequency filter	s	0.01
Frequency droop	p.u.	0.05

The GFL is connected to the 230-kV bus with a 13.8/230-kV delta/grounded wye transformer rated at 200 MVA. The initial commanded real output of the inverter is 91.8 MW to establish a steady-state frequency of 60 Hz; the additional 1.8 MW covers the SC consumption and the transformers/line losses. The reactive power output set point is set at 3 Mvar to compensate for energizing the interfacing transformer.

C. Short-Circuit Ratio

The short circuit ratio (SCR), as used for assessing the strength/voltage stiffness of a particular interconnection point in a power system prior to the integration of a power electronic power source, is defined as shown in (1) [9]. Here, S_{SCMVA} is the short-circuit MVA at the interconnection point, and P_{RMW} is the megawatt rating of the renewable source. Generally, a relatively lower SCR indicates a weak point in the power system, with values less than three considered low [9].

$$SCR = \frac{S_{SCMVA}}{P_{RMW}} \quad (1)$$

The SCR was calculated in this system by first measuring the short-circuit fault current from the SC at the GFL point of common coupling for the varying transmission line lengths. The single-phase root mean square current was then used in $S_{SCMVA} = \sqrt{3} I_{phase} V_{LL}$ to arrive at a value for S_{SCMVA}. Assuming the ability to output a real power equal to the apparent power rating of the GFL inverter, P_{RMW} is taken as 150 MW. The resultant SCRs for the varying transmission line lengths are given in Table IV.

TABLE IV
SCR AT GFL BUS FOR VARYING LINE LENGTHS

Line Length (km)	SCR
25	3.98
75	3.40
125	2.97

D. Simulations Performed

The simulations performed for this work are outlined as follows:

1) Load step sensitivities: 10% load increase with varied parameters, line length = 25 km:
   - Inverter response times: 50 ms, 150 ms, 250 ms
   - Frequency deadband: 1 mHz, 10 mHz, 100 mHz
   - Inertia constant: 2 s, 4 s, 6 s
2) Six-cycle, balanced, bolted fault: varied transmission line length:
   - Line length: 25 km, 75 km, 125 km
3) Six-cycle, unbalanced faults: varied transmission line length:
   - Line length: 25 km, 75 km, 125 km
   - Fault type: L-G, L-L-G, L-L

IV. RESULTS

The following are the results of the simulations, as outlined in Section III-D.

A. Steady State

The system is initialized by first operating the SC as an ideal voltage source before releasing the machine and exciter at 0.5 s and 1.0 s, respectively. Brief oscillations in frequency and voltage, of rate and magnitude common to the release of most machines in PSCAD simulations, occur with sufficient damping following the release. For a transmission line length of 25 km, the system achieves stability at 60 Hz with no oscillations in the the outputs of the GFL inverter or SC. The system is similarly stable for line lengths of 75 and 125 km. If the line length is increased to 150 km, however, the system is unstable because the oscillations following the machine/exciter release increase without bound. Note that the SCR for this line length will be well below three. To be thorough, after releasing the SC and allowing the oscillations to diminish, the SC was disconnected. As expected, the system rapidly deenergizes.

B. Load Step Sensitivity

Following are the results of the sensitivity studies for the 10% load step for variations in the parameters: response time of the GFL ($T_{response}$), frequency droop deadband ($f_{deadband}$), and the inertia constant (H) of the SC. Only one parameter is varied at a time. When not being varied, the following are kept constant: $T_{response} = 50ms$, $f_{deadband} = 1mHz$, and $H = 2s$. The line length for all sensitivity simulations is maintained at 25 km.

1) Inverter Response Time: Fig. 5 presents the real power output of the GFL and the SC as well as the frequency of the SC following a 10% load step. Three simulation results are presented: those of response times of $250ms$, $150ms$, and $50ms$. Broadly, by comparing these three sets of traces from the load step, the process by which the system reacts to a load step is evident. Initially, the load step impacts the SC, as shown by the shift to a sourcing of real power immediately following the load step. Because of the rotational dynamics of the SC, this results in a decrease in frequency. As this frequency decline is sensed by the GFL, the real power output is modulated in accordance with the frequency droop control. The decline is arrested when the real power output modulation of the GFL covers the additional load.

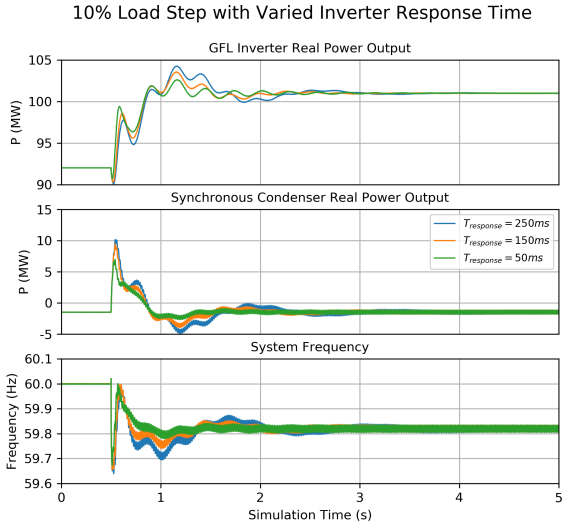

Fig. 5. Real power response of the GFL and SC with the bus frequency following a 10% load step. GFL response time is varied.

For all three response time settings, the settling frequency and real power outputs converge to the same final values. The change in response time largely results in a deeper nadir for larger response times and prolonged oscillations following the load step. Although the slower oscillations do diminish, there are persistent, 60-Hz oscillations in the frequency and real power outputs, as shown in Fig. 6. That these oscillations are in both the real power outputs and frequency is sensible considering the linkage of the three; when the SC is consuming less than the steady-state value, the frequency declines, and vice versa. That the GFL and frequency oscillations are in phase

is counterintuitive to the frequency droop relation because a higher frequency will result in a decreased output signal. This could indicate that the phase response of the GFL and propagation delay across the transmission line yields a near 180-degree displacement. Although the change in response time ought to change to this phase separation, Fig. 6 does not corroborate this. Further investigation is required.

Changing the load from a constant power type (which is modeled in PSCAD by modulating the impedance after each cycle to maintain the desired consumption) to a constant impedance has a minimal effect on these oscillations. An open question with respect to the feasibility of this system is whether these oscillations are acceptable. In these simulations, the GFL oscillations are a magnitude of 50 kW, or 0.05% of the total output, whereas the SC oscillations are 500 kW. It is not immediately clear why the SC oscillations are an order of magnitude larger than the GFL oscillations.

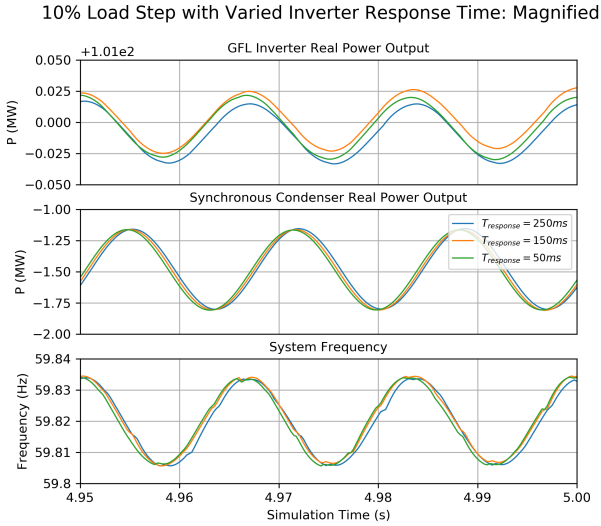

Fig. 6. Real power/frequency oscillations after initial load step transients diminish.

The SC reactive power output and bus voltage are shown in Fig. 7. The load step results in a decrease in the bus voltage, which is met by a corresponding increase in reactive power output of the SC. Oscillations occur, but they are damped. Persistent, 60-Hz oscillations are present in the settled values, with a 600-kVar magnitude in the reactive power oscillations and a 100-V magnitude in the oscillations of the 230-kV bus.

2) Inverter Frequency Deadband: Changing the frequency deadband of the frequency droop implementation resulted in no significant changes in either the real power output of the GFL or the frequency of the system. This changes if the transmission line is removed, creating a single bus. In this case, the deadband corresponds to an in-kind decrease in the settling frequency of the system following a load step.

3) Inertia: The results of changing the SC inertia constant and simulating the 10% load step are shown in Fig. 8. The results are as expected. By increasing the inertia constant of

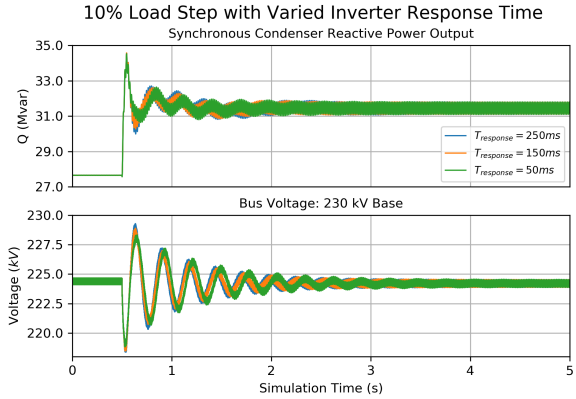

Fig. 7. SC reactive power output and bus voltage following a 10% load step with different GFL response times.

the SC, a larger amount of kinetic energy is present, which decreases the initial rate of change of frequency of the SC following the load step. As a result, the frequency change at the GFL bus is delayed, and therefore the response of the GFL is prolonged. The settling frequencies are all the same, and the resultant 60-Hz oscillations are still present. In short, increasing the inertia reduces the volatility of the frequency, a well-known result for power systems operating within inertial characteristics.

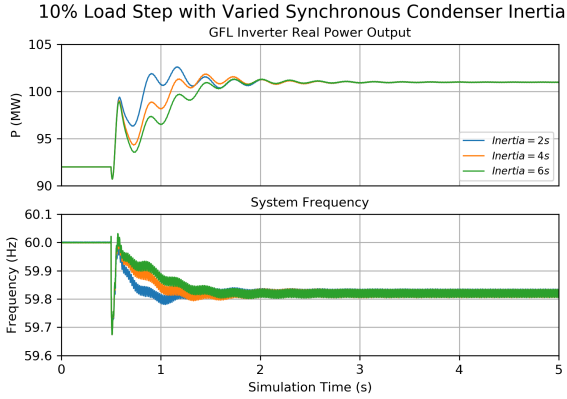

Fig. 8. Real power output of GFL inverter with system frequency following a 10% load step for variations in the synchronous condenser inertia constant.

C. Balanced Fault Response

The following results are for a three-phase, bolted fault at the SC bus that persists for six cycles. The first set of results, presented in Figs. 9 and 10, are the response to the fault with the frequency droop enabled and the following parameters: $T_{response} = 50ms$, $f_{deadband} = 1mHz$, and $s = 2$. Three simulations were performed for three different line lengths: 25 km, 75 km, and 125 km. The SCRs at the GFL inverter for these three line lengths are given in Table IV.

Fig. 9 provides the real power output of the GFL and SC as well as the system frequency. The GFL output shows a

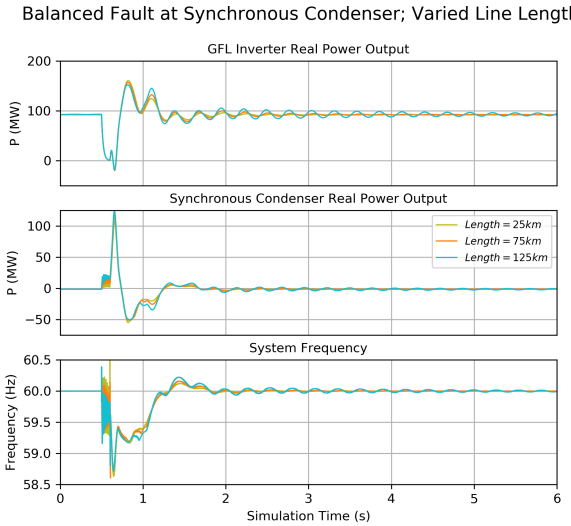

Fig. 9. Real power output of GFL inverter and system frequency response to a six-cycle fault with varying line lengths.

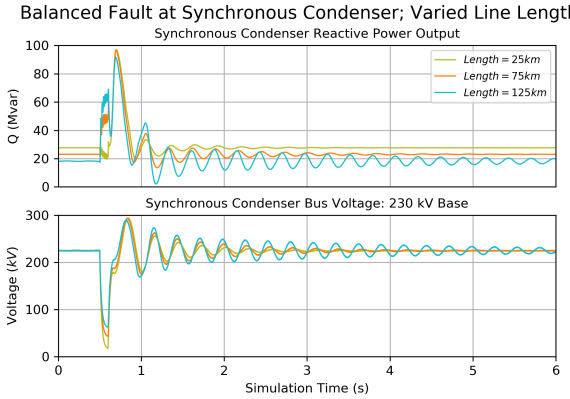

Fig. 10. Synchronous condenser reactive power output and bus voltage response to a six-cycle fault with varying line lengths.

decrease to zero output during the fault, a result of the near-zero voltage during the faulted state. The output rapidly returns after the fault is cleared and increases substantially because of the decrease in frequency. The real power output of the SC is similarly near zero during the fault before sourcing a very large amount of real power immediately after the clearing. This sourcing of power decreases the frequency, supplying the signal to the GFL to modulate the real power output. The oscillations in the frequency immediately during the fault are likely a computational anomaly because of the calculation of frequency with a phase-locked loop when the voltage is near zero. Generally, the increase in line length does not produce significant changes to the initial transients although the damping of the oscillations decreases with line length. Although truncated in the figure, the oscillations decrease to zero as the simulation progresses for a longer time.

The reactive power output and bus voltage of the SC are provided in Fig. 10. The SC reactive power output increases during the fault for the longer transmission lines although the peak outputs are all similar. Again, the damping of the oscillations is decreased for longer transmission lines although the oscillations do eventually diminish. The voltage profile is not exceptional; because of the near-zero impedance of the fault, this decreases to near zero during the fault. The overvoltage after the fault is cleared reaches near 300 kV. Not modeled in this work is any overvoltage tripping of the GFL.

D. Unbalanced Fault Responses

In testing the response to unbalanced faults, both the type of fault and the length of the line were adjusted. Three types of faults, L-G, L-L-G, and L-L were tested. The previously used line lengths, 25 km, 75 km, and 125 km were used. The results of these simulations are summarized in Table V.

The fault transients with respect to the measured quantities of voltage, frequency, and power outputs, are not substantially different from those viewed for the balanced faults in Figs. 9 and 10. As such, they are not presented graphically. All cases, for the different line lengths and various types of faults, ultimately reach a steady state.

TABLE V
UNBALANCED FAULT RESULTS, TD: TRANSIENTS DIMINISH

	Line Length (km)		
Fault Type	25	75	125
L - G	TD	TD	TD
L - L - G	TD	TD	TD
L - L	TD	TD	TD

V. CONCLUSION

A simple system comprising a SC with a collocated load, a GFL with frequency droop functionality, and a single connecting Bergeron model transmission line was perturbed with 10% load steps and a variety of faults to assess the transient stability. The system was initialized at 60 Hz, with the inverter covering all active power consumption under the assumption that a SG would have been used to achieve this initial steady state. This operational point is applicable to a power system with very high renewable energy penetrations, where the preferred operation is to remove the SGs during high renewable availability because of the minimum generation constraints of the SGs negatively impacting the peak penetration. Ample headroom was assumed for the inverter.

A surprising level of stability was observed for transmission line lengths up to 125 km. Following load steps of 10% with a line length of 25 km, the system rapidly converges to a new steady state. Changing the GFL response time, frequency deadband, or inertia constant of the SC influences the path to this new steady state, but it does not influence the final settling conditions. An interesting relic of the load step is the presence of 60-Hz oscillations in the real and reactive powers and the linked voltage frequency. Whether these oscillations exceed operational acceptance is not explored in this work. Six-cycle, three-phase bolted faults at the SC result in anticipated transients in the outputs of the SC and inverter, but the system

returns to the initial steady state. For longer transmission lines, the damping of oscillations decreases, but still ultimately diminishes for the line lengths investigated. Similarly for unbalanced faults, the system recovers to a steady state for line lengths up to 125 km.

Although the simplicity of the model is questionable with application to existing power systems, the results of this study indicate that an SC and a GFL, feasibly operating at a 100% instantaneous renewable penetration, *may potentially* yield a power system capable of withstanding standard perturbations. Recognizing that this study is not a comprehensive analysis of this potential system and further research is required, necessary next steps should include:

- a comprehensive small-signal analysis of these two devices
- higher fidelity modeling of the inner controller loops of the GFL and passive filters in EMT simulations
- automatic voltage regulator modeling for the SC, as opposed to a proportional support mechanism
- small signal and transient simulations with larger, more complex transmission systems under varying power flows

This study has provided an impetus to further investigate the use of these two power system devices to create a functional power system during periods of surplus renewable energy availability.

VI. Acknowledgments

This work was authored by the National Renewable Energy Laboratory, operated by Alliance for Sustainable Energy, LLC, for the U.S. Department of Energy (DOE) under Contract No. DE-AC36-08GO28308. This material is based upon work supported by the U.S. Department of Energys Office of Energy Efficiency and Renewable Energy (EERE) under Solar Energy Technologies Office (SETO) Agreement Number 34224. The views expressed in the article do not necessarily represent the views of the DOE or the U.S. Government. The U.S. Government retains and the publisher, by accepting the article for publication, acknowledges that the U.S. Government retains a nonexclusive, paid-up, irrevocable, worldwide license to publish or reproduce the published form of this work, or allow others to do so, for U.S. Government purposes.

References

[1] J. A. Taylor, S. V. Dhople, and D. S. Callaway, "Power systems without fuel," *Renewable and Sustainable Energy Reviews*, vol. 57, pp. 1322 – 1336, 2016. [Online]. Available: http://www.sciencedirect.com/science/article/pii/S1364032115014665

[2] B. Kroposki, B. Johnson, Y. Zhang, V. Gevorgian, P. Denholm, B. Hodge, and B. Hannegan, "Achieving a 100% Renewable Grid: Operating Electric Power Systems with Extremely High Levels of Variable Renewable Energy," *IEEE Power and Energy Magazine*, vol. 15, no. 2, pp. 61–73, Mar. 2017.

[3] F. Milano, F. Dörfler, G. Hug, D. J. Hill, and G. Verbi, "Foundations and Challenges of Low-Inertia Systems," in *2018 Power Systems Computation Conference (PSCC)*, Jun. 2018, pp. 1–25.

[4] U. Markovic, O. Stanojev, E. Vrettos, P. Aristidou, and G. Hug, "Understanding Stability of Low-Inertia Systems," Feb. 2019. [Online]. Available: https://doi.org/10.31224/osf.io/jwzrq

[5] A. Ulbig, T. S. Borsche, and G. Andersson, "Impact of Low Rotational Inertia on Power System Stability and Operation," *IFAC Proceedings Volumes*, vol. 47, no. 3, pp. 7290–7297, Jan. 2014.

[6] Y. Liu, S. Yang, S. Zhang, and F. Z. Peng, "Comparison of synchronous condenser and STATCOM for inertial response support," in *2014 IEEE Energy Conversion Congress and Exposition (ECCE)*, Sep. 2014, pp. 2684–2690.

[7] Y. Liu, Y. Yu, C. Wang, Z. Zou, C. Jiang, C. Sun, and J. Yu, "Review on Synchronous Condenser Modeling Study," in *2018 China International Conference on Electricity Distribution (CICED)*, Sep. 2018, pp. 227–232.

[8] A. Stiger, R. A. Rivas, and M. Halonen, "Synchronous Condensers Contribution to Inertia and Short Circuit Current in Cooperation with STATCOM," in *2019 IEEE PES GTD Grand International Conference and Exposition Asia (GTD Asia)*, Mar. 2019, pp. 955–959.

[9] M. Osman, N. Segal, A. Najafzadeh, and J. Harris, "Short Cicuit Modeling and System Strength," North American Electric Reliability Corporation, Atlanta, GA, White Paper, Feb. 2018.

[10] P. Piagi and R. H. Lasseter, "Autonomous control of microgrids," in *2006 IEEE Power Engineering Society General Meeting*, Jun. 2006, pp. 1–8.

[11] H. Beck and R. Hesse, "Virtual Synchronous Machine," in *2007 9th International Conference on Electrical Power Quality and Utilisation*, Oct. 2007, pp. 1–6.

[12] B. Johnson, M. Rodriguez, M. Sinha, and S. Dhople, "Comparison of Virtual Oscillator and Droop Control," in *2017 IEEE 18th Workshop on Control and Modeling for Power Electronics (COMPEL)*, Jul. 2017, pp. 1–6.

[13] R. W. Kenyon, E. T. Hale, C. Barrows, and B. M. Hodge, "Managing Solar Photovoltaic Integration in the Western United States: Power Electronic Converter Influences on Power System Control and Stability: A Primer," National Renewable Energy Laboratory, Tech. Rep. NREL/TP-5D00-72964, Forthcoming.

[14] S. Kalsi, D. Madura, and M. Ross, "Performance of Superconductor Dynamic Synchronous Condenser on an Electric Grid," in *2005 IEEE/PES Transmission Distribution Conference Exposition: Asia and Pacific*, Aug. 2005, pp. 1–5.